

Light Scattering by Cylindrical Fibers with High Aspect Ratio Using the Null-Field Method with Discrete Sources

Sorin Pulbere*, Thomas Wriedt**

(Received: 7 March 2003, in revised form: 12 November 2003, accepted: 14 April 2004)

Abstract

The problem of computing light scattering by cylindrical fibers with high aspect ratio in the framework of the Null-Field method with discrete sources is treated. Numerical experiments for investigating the scattering

properties of two fiber geometries are performed using distributed spherical vector wave functions as discrete sources.

Keywords: fiber characterization, Null-Field method

1 Introduction

Light scattering by finite cylindrical particles is of interest in optical particle characterization in order to develop techniques for the detection and characterization of airborne fibers.

Asbestos, mineral and glass fibers have been widely utilized, especially as insulating materials in construction and other high temperature applications. Due to corrosion and other phenomena, fibers may become airborne. Airborne fibers are considered to cause serious health hazards, depending on their material and geometrical properties [1]. The standard procedure for detection of airborne fibers is based on collecting them with a special filter, and classifying them under a scanning electron microscope with the human eye. This procedure is, of course, time-consuming as well as expensive, since trained personnel have to detect the fibers and differentiate between the harmful and harmless ones. Another problem arising is accuracy, as found by Höfert et al. [2]. The use of different laboratories to measure fiber concentration for one fiber probe, led to very different results, and there were even differences of up to 40% in the calculated concentrations of reference estimations performed by four laboratories. Since this method is

quite laborious, there is much interest in developing an online optical method for fiber characterization. In previous work, it was possible to develop fiber detectors based on light scattering, though this method still requires further improving [3–5]. In order to develop such an instrument, light scattering computations are needed. There are various methods in existence to compute scattering by a finite fiber, but they commonly fail with fibers having an aspect ratio larger than about 10.

The **T**-matrix method has been widely recognized as a powerful theoretical tool to compute light scattering from finite cylinders. Yet, despite this, computation investigations show that simulation of scattering by the **T**-matrix method is possible only for particles with quite a small aspect ratio [6]. Other methods also encounter problems with particles having a high aspect ratio. The recently developed Discrete Sources Method has been extended to compute scattering by highly elongated particles [7].

A number of modifications to the conventional method have been suggested to improve the numerical stability. One of these formal modifications is the Null-Field method with discrete sources developed within our group [8]. Essentially, in this method different types of discrete sources are used for approximating the surface current densities on the exterior surface of the scattering particle. The discrete sources are placed on a certain support in a region additional to that where the solution is required.

The unknown amplitudes of discrete sources that produce the surface current densities, are computed by

* Dipl.-Ing. S. Pulbere, University of Bremen, Chemical Engineering, Badgasteiner Str. 3, 28359 Bremen (Germany). E-mail: pulbere@iwt.uni-bremen.de

** Dr.-Ing. T. Wriedt, University of Bremen, Institut für Werkstofftechnik, Badgasteiner Str. 3, 28359 Bremen (Germany).

using the null-field condition for the total electric field on the particle surface.

The aim of the present contribution is to demonstrate that the transition matrix can be computed for elongated cylinders with high aspect ratio, in the framework of the Null-Field method with discrete sources. The influence of small geometry variations at the cylinder end, on the scattering diagrams, is also investigated.

2 Null-Field Method with Discrete Sources

Since a full theoretical outline of the Null-Field method with discrete sources has been published previously [8], this paper will only briefly summarize the theory. Some of the special features that should be applied in the case of elongated particles with very high aspect ratio are also discussed.

We denote the domain contained inside the cylinder with D_i and the space outside with D_s . The fiber surface is denoted by S in Figure 1.

Given \mathbf{E}_0 and \mathbf{H}_0 , in order to find a complete solution to the Maxwell equations representing an incident electromagnetic field, it is necessary to compute the scattered vector fields $\mathbf{E}_s, \mathbf{H}_s$ in the free space, and $\mathbf{E}_i, \mathbf{H}_i$ inside the scatterer, satisfying the reduced Maxwell equations:

$$\nabla \times \mathbf{E}_t = jk_t \mu_t \mathbf{H}_t,$$

$$\nabla \times \mathbf{H}_t = -jk_t \varepsilon_t \mathbf{E}_t \text{ in } D_t, t = s, i, \quad (1)$$

as well as the transmission conditions on the particle boundary:

$$\mathbf{n} \times \mathbf{E}_i = \mathbf{n} \times \mathbf{E}_0 + \mathbf{n} \times \mathbf{E}_s,$$

$$\mathbf{n} \times \mathbf{H}_i = \mathbf{n} \times \mathbf{H}_0 + \mathbf{n} \times \mathbf{H}_s, \quad (2)$$

In addition, the scattered fields \mathbf{E}_s and \mathbf{H}_s must satisfy the Silver-Müller radiation condition for all directions $\frac{x}{|x|}$

$$\frac{x}{|x|} \times \mathbf{H}_s + \mathbf{E}_s = o\left(\frac{1}{|x|}\right) \quad (3)$$

as $|x| \rightarrow \infty$.

In order to solve the transmission boundary-value problem in the framework of the Null-Field method with discrete sources, the scattering object is replaced by a set of surface current densities \mathbf{e} and \mathbf{h} , so that the sources and the fields in the exterior region are exactly the same as those existing in the original scattering problem.

A set of integral equations for the surface current densities \mathbf{e} and \mathbf{h} , is derived for a set of distributed lowest-

order vector spherical functions used as discrete sources, ensuring the best convergence for fibers with very large aspect ratios.

The set of distributed lowest-order vector spherical functions is described by:

$$\{\mathcal{M}_{mn}^{1,3}, \mathcal{N}_{mn}^{1,3}\}_{m \in \mathbb{Z}, n=1,2,\dots},$$

with

$$\mathcal{M}_{mn}^{1,3}(\mathbf{x}) = \mathcal{M}_{m,|n|+l}^{1,3}(\mathbf{x} - z_n \mathbf{e}_3),$$

$$\mathcal{N}_{mn}^{1,3}(\mathbf{x}) = \mathcal{N}_{m,|n|+l}^{1,3}(\mathbf{x} - z_n \mathbf{e}_3), \quad (4)$$

where (z_n) is a bounded sequence on a segment of the z -axis.

Essentially the Null-Field method with discrete sources consists of the projection relationship:

$$\int_S \left[(\mathbf{e} - \mathbf{e}_0) \cdot \mathcal{M}_{-mn}^3 + j \sqrt{\frac{m_s}{\varepsilon_s}} (\mathbf{h} - \mathbf{h}_0) \cdot \mathcal{N}_{-mn}^3 \right] dS = 0, \quad (5)$$

$$\int_S \left[(\mathbf{e} - \mathbf{e}_0) \cdot \mathcal{N}_{-mn}^3 + j \sqrt{\frac{m_s}{\varepsilon_s}} (\mathbf{h} - \mathbf{h}_0) \cdot \mathcal{M}_{-mn}^3 \right] dS = 0,$$

with $m = m_{\max}, \dots, m_{\max}, n = 1, \dots, n_{\max}$.

The surface current densities are approximated by fields of discrete sources. There is a sequence $\{a_{mn}, b_{mn}\}$ such that:

$$\begin{pmatrix} \mathbf{e} \\ \mathbf{h} \end{pmatrix} = \sum_{m=-m_{\max}}^{m_{\max}} \sum_{n=1}^{n_{\max}} a_{mn} \begin{pmatrix} \mathbf{n} \times \mathcal{M}_{mn}^1 \\ -j \sqrt{\frac{\varepsilon_i}{\mu_i}} \mathbf{n} \times \mathcal{N}_{mn}^1 \end{pmatrix} + b_{mn} \times \begin{pmatrix} \mathbf{n} \times \mathcal{N}_{mn}^1 \\ -j \sqrt{\frac{\varepsilon_i}{\mu_i}} \mathbf{n} \times \mathcal{M}_{mn}^1 \end{pmatrix}. \quad (6)$$

In the above formulation, the approximated surface current densities and the null-field condition are expressed in terms of distributed lowest-order spherical vector wave functions.

Consequently, the matrix system includes Hankel functions of low orders, which generate a better-conditioned system of equations compared to that obtained in the single spherical coordinate-base Null-Field Method. The use of lowest-order spherical multipoles is most effective for axisymmetric particles. By using a system of lowest-order spherical vector wave functions distributed along the axis of revolution, it is possible to reduce the original problem to a sequence of subproblems for each azimuthal mode. Therefore, this presents a way to analytically

deal with the later computer code convergence problems.

Once the surface current densities \mathbf{e} and \mathbf{h} are determined, the scattered field outside the circumscribing sphere is obtained by using the representation theorem, which describes the scattered field as a series of radiating spherical vector wave functions:

$$\mathbf{E}_s = \sum_{v=1}^{\infty} f_v \mathbf{M}_v^3 + g_v \mathbf{N}_v^3, \quad (7)$$

$$\mathbf{H}_s = -j \sqrt{\frac{\epsilon_s}{\mu_s}} \sum_{v=1}^{\infty} f_v \mathbf{M}_v^3 + g_v \mathbf{N}_v^3, \quad (8)$$

with expansion coefficients:

$$f_v = \frac{jk_s^2}{\pi} \int_S \left[\mathbf{e} \cdot \mathbf{N}_v^1 + j \sqrt{\frac{\mu_s}{\omega_s}} \mathbf{h} \cdot \mathbf{M}_v^1 \right] dS, \quad (9)$$

$$g_v = \frac{jk_s^2}{\pi} \int_S \left[\mathbf{e} \cdot \mathbf{M}_v^1 + j \sqrt{\frac{\mu_s}{\omega_s}} \mathbf{h} \cdot \mathbf{N}_v^1 \right] dS,$$

where $v = (m, n)$ and $\bar{v} = (-m, n)$.

In order to derive the \mathbf{T} -matrix, it must be assumed that the incident field inside a bounded domain containing S , can be expressed as a series of vector spherical wave functions:

$$\mathbf{E}_0 = \sum_{v=1}^{\infty} a_v^0 \mathbf{M}_v^1 + b_v^0 \mathbf{N}_v^1, \quad (10)$$

$$\mathbf{H}_0 = -j \sqrt{\frac{\epsilon_s}{\mu_s}} \sum_{v=1}^{\infty} a_v^0 \mathbf{N}_v^1 + b_v^0 \mathbf{M}_v^1.$$

Consequently, the relationship between the scattered and the incident field coefficients is linear and is given by a transition matrix \mathbf{T} as follows:

$$\begin{bmatrix} f_v \\ g_v \end{bmatrix} = \mathbf{T} \begin{bmatrix} a_v^0 \\ b_v^0 \end{bmatrix}. \quad (11)$$

Here,

$$\mathbf{T} = \mathbf{B} \mathbf{A}^{-1} \mathbf{A}_0, \quad (12)$$

where \mathbf{A} , \mathbf{B} and \mathbf{A}_0 are block matrices written in the general form as:

$$\mathbf{X} = \begin{bmatrix} X_{v\mu}^{11} & X_{v\mu}^{12} \\ X_{v\mu}^{21} & X_{v\mu}^{22} \end{bmatrix}, v, \mu = 1, 2, \dots, \quad (13)$$

with \mathbf{X} standing for \mathbf{A} , \mathbf{B} and \mathbf{A}_0 . The elements of the matrices \mathbf{A} , \mathbf{B} and \mathbf{A}_0 are presented in the appendix.

The elements of the \mathbf{T} -matrix are independent of the incident and scattered fields and depend only on the shape, size parameter and refractive index of the scattering particle, as well as on its orientation with respect to the coordinate system. Consequently, the \mathbf{T} -matrix needs to be computed only once, and then this value can be used in computations for any direction of light incidence and scattering.

3 Numerical Results

The formulation presented in Sec. 2 has been implemented in a computer program. In this section, two types of cylindrical fiber geometry, are considered. Though, in reality, a variety of cylinder end types appear, the computations are restrained only to some axisymmetric geometries and therefore, it is not possible to perform light scattering simulations for more realistic “broken” cylinders. The first type is represented by a straight cut end cylinder with the half-length b , and radius a , as in Figure 1. The second fiber type is represented by a cylindrical structure which has hemispheres added at the ends. This rounded end cylinder has a total half-length b , and radius a .

The origin O , of the coordinate system is positioned in the center of the cylindrical fiber, with the z -axis corresponding to the symmetry axis of the scatterer, and angle θ defined with respect to the z -axis, as in Figure 2. Every point M on the surface S , is described by a vector \mathbf{r} of length r and derivative dr :

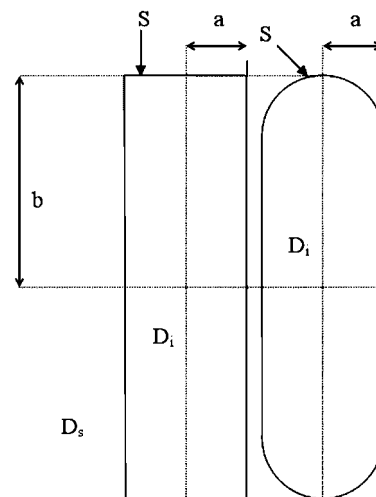


Fig. 1: Geometry of elongated cylinders with straight-cut ends and with rounded ends.

$$\begin{aligned}
r &= \frac{b}{\cos \theta} & dr &= \frac{b \sin \theta}{\cos^2 \theta}, & 0 < \theta < \tan^{-1} \frac{a}{b} \\
r &= \frac{a}{\sin \theta} & dr &= \frac{-a \cos \theta}{\sin^2 \theta}, & \tan^{-1} \frac{a}{b} < \theta < \tan^{-1} \frac{-a}{b} \\
r &= \frac{-b}{\cos \theta} & dr &= \frac{-b \sin \theta}{\cos^2 \theta}, & \tan^{-1} \frac{-a}{b} < \theta < \pi
\end{aligned} \quad (14)$$

for the straight-cut end cylinder, and:

$$\begin{aligned}
r &= b \cos \theta + \sqrt{a^2 - b^2 \sin^2 \theta} \\
dr &= -b \sin \theta - \frac{b^2 \cos \theta \sin \theta}{\sqrt{a^2 - b^2 \sin^2 \theta}}, & 0 < \theta < \tan^{-1} \frac{a}{b} \\
r &= \frac{a}{\sin \theta} & dr &= \frac{-a \cos \theta}{\sin^2 \theta}, & \tan^{-1} \frac{a}{b} < \theta < \tan^{-1} \frac{-a}{b} \\
r &= -b \cos \theta + \sqrt{a^2 - b^2 \sin^2 \theta} \\
dr &= b \sin \theta - \frac{b^2 \cos \theta \sin \theta}{\sqrt{a^2 - b^2 \sin^2 \theta}}, & \tan^{-1} \frac{-a}{b} < \theta < \pi
\end{aligned} \quad (15)$$

for the rounded end cylinder. The wave number of the region D_i is $k_i = k(\epsilon_i \mu_i)^{\frac{1}{2}}$, while the wave number for the free space is $k_s = k(\epsilon_i \mu_i)^{\frac{1}{2}}$, where $k = \frac{\omega}{c}$.

For simplicity, it is assumed that the incident wave is a plane wave traveling perpendicular to the symmetry axis of the cylinder. The polarization direction encloses the angle α_{pol} with the x -axis.

The perfect scatterers considered, consist of elongated cylinders with refractive indices, $m = 1.5$, and aspect ratio between 1:10 and 1:50.

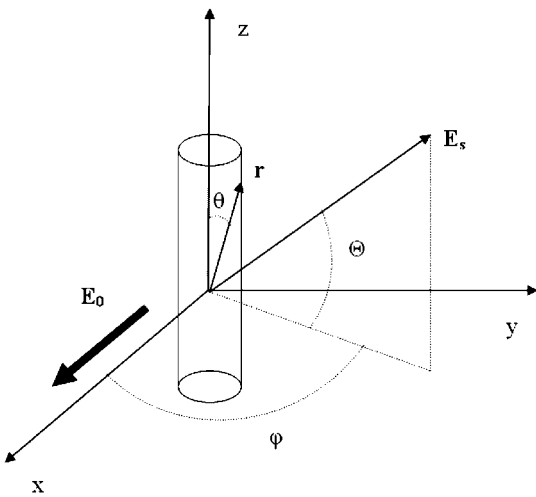


Fig. 2: Description of the coordinate system.

Specifically, the differential scattering cross section (DSCS), normalized by πb^2 , will be computed in the azimuthal plane, $\varphi = 0^\circ$, for parallel and perpendicular polarization of the incident wave with respect to the scattering angle θ :

$$\frac{\sigma_d}{\pi b^2} = \frac{|k_s E_{s0}^N|^2}{\pi |k_s b|^2}. \quad (16)$$

In the first example presented in Figure 3, a rounded end cylinder with aspect ratio 1:10 is considered. In this case, a collection of sources located on the symmetry axis of the scatterer was utilized. To verify the results, a check against MMP (multiple multipole method) simulations was found to yield very good agreement [9, 10]. The shift between the two curves is caused by different methods of normalization.

In the next example presented in Figure 4, a straight-cut end cylinder with aspect ratio 1:50 is considered. Although for such a large aspect ratio, other methods fail to converge, the Null-Field method with discrete sources still gives a good convergence test result. This was especially possible due to the use of the extended-precision variables utilized in the computation of the transfer matrix. The higher variable precision improves the algorithm stability, and therefore, it is possible to compute the light scattering from cylinders with very high aspect ratio.

The exact geometry of the cylinder end may seem unimportant for practical purposes, but to evaluate the results from experimental measurements on straight-cut end cylinders, it is of great interest to have appropriate simulation curves. In this respect, a comparison between

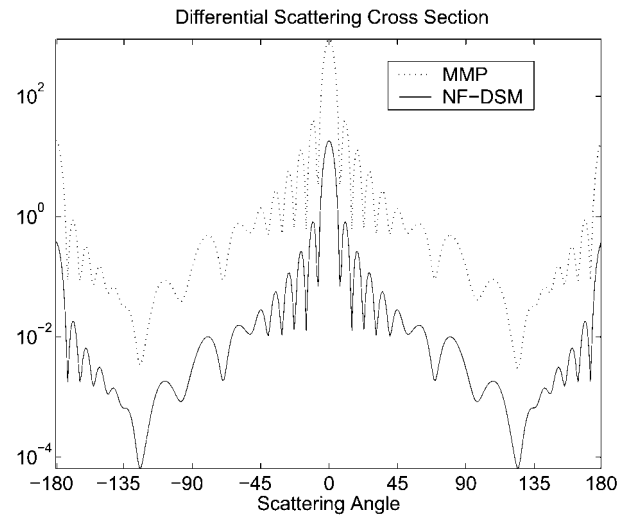


Fig. 3: Rounded-end cylinder with $kb = 8\pi$, aspect ratio 1:10 and $m = 1.5$. (Parallel polarization).

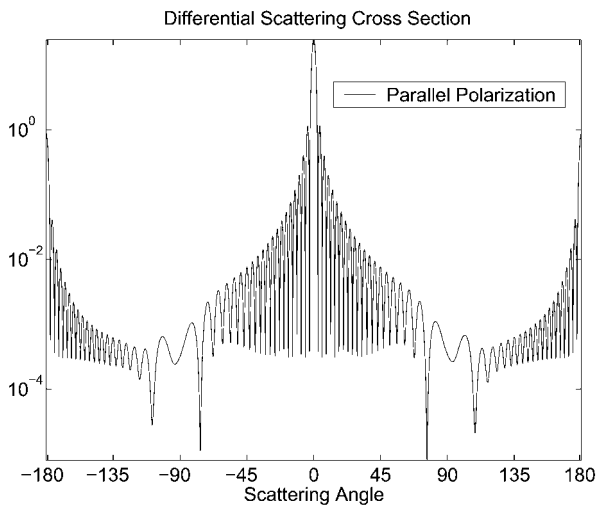


Fig. 4: Differential scattering cross section for a straight-cut end cylinder with an aspect ratio 1:10, $kb = 20\pi$ and $m = 1.5$. (Parallel polarization).

the scattering pattern obtained for a straight-cut end, and a rounded end cylinder in both perpendicular and parallel polarizations, was performed.

In Figure 5, the DSCS is computed for particles with an aspect ratio of 1:30, for parallel polarization. It is observed that, while in forward scattering, at small angles there is not a major difference between the two curves, at larger angles the differences are significant, and may thus lead to misinterpretation in the evaluation of experimental results. As an intuitive assessment, one may think that for large fibers, with very high aspect ratio, the type of fiber end may be unimportant. Although it is not possible to perform light scattering simulations by real-shape broken fibers, the differences that appear between the scattering diagrams for straight-cut end and rounded end cylinders allows one to state that the type of fiber end plays a major role in the scattering features, irrespective of the fiber dimensions and aspect ratio.

Although in the case of parallel polarization, it is still possible to find a correspondence between the scattering diagrams for two cylinders that have the same length, if the scattering diagrams for perpendicular polarization in Figure 3 are analyzed, the differences between the two curves are much larger, again demonstrating the importance of the cylinder end type, Figure 6.

4 Conclusions

An application of the Null-Field method with discrete sources to compute light scattering by elongated cylindrical fibers, which is able to resolve problems for aspect

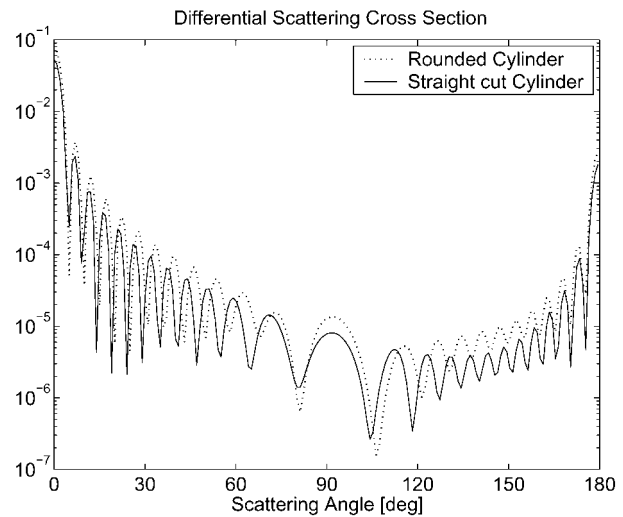


Fig. 5: Comparison between a straight-cut end cylinder and a rounded-end cylinder with an aspect ratio 1:30, $kb = 12\pi$ and $m = 1.5$. (Parallel polarization).

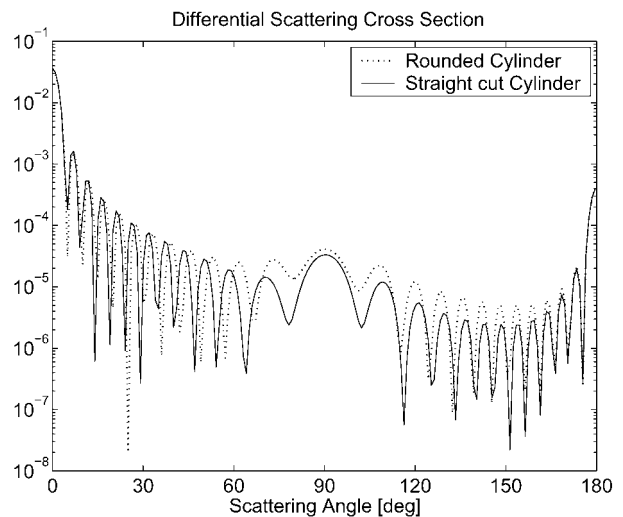


Fig. 6: Comparison between a straight-cut end cylinder and a rounded-end cylinder with an aspect ratio 1:30, $kb = 12\pi$ and $m = 1.5$. (Perpendicular polarization).

ratios up to 1:50 by using the actual programs, was presented. This is an important step forward that should lead to a better interpretation of experimental measurements. It was also demonstrated that the exact geometry of the cylinder end has a large influence on the scattering curves, even at high aspect ratios.

A further paper will be devoted to investigating the validity of the Fraunhofer Diffraction Theory, by comparisons to the Null-Field method with discrete sources. This work was performed in connection with the development of an airborne cylindrical fiber detector, based on laser light scattering.

5 Appendix

The block elements of matrices \mathbf{A} , \mathbf{B} and \mathbf{A}_0 are given by:

$$\begin{aligned}
 A_{v\mu}^{11} &= \int_S \left[(\mathbf{n} \times \mathcal{M}_\mu^1) \cdot \mathcal{M}_v^3 + \sqrt{\frac{\varepsilon_i}{\varepsilon_s}} (\mathbf{n} \times \mathcal{N}_\mu^1) \cdot \mathcal{N}_v^3 \right] dS, \\
 A_{v\mu}^{12} &= \int_S \left[(\mathbf{n} \times \mathcal{N}_\mu^1) \cdot \mathcal{M}_v^3 + \sqrt{\frac{\varepsilon_i}{\varepsilon_s}} (\mathbf{n} \times \mathcal{M}_\mu^1) \cdot \mathcal{N}_v^3 \right] dS, \\
 A_{v\mu}^{21} &= \int_S \left[(\mathbf{n} \times \mathcal{M}_\mu^1) \cdot \mathcal{N}_v^3 + \sqrt{\frac{\varepsilon_i}{\varepsilon_s}} (\mathbf{n} \times \mathcal{N}_\mu^1) \cdot \mathcal{M}_v^3 \right] dS, \\
 A_{v\mu}^{22} &= \int_S \left[(\mathbf{n} \times \mathcal{N}_\mu^1) \cdot \mathcal{N}_v^3 + \sqrt{\frac{\varepsilon_i}{\varepsilon_s}} (\mathbf{n} \times \mathcal{M}_\mu^1) \cdot \mathcal{M}_v^3 \right] dS,
 \end{aligned} \tag{17}$$

$$\begin{aligned}
 B_{v\mu}^{11} &= \frac{jk_s^2}{\pi} \int_S \left[(\mathbf{n} \times \mathcal{M}_\mu^1) \cdot \mathbf{N}_v^1 + \sqrt{\frac{\varepsilon_i}{\varepsilon_s}} (\mathbf{n} \times \mathcal{N}_\mu^1) \cdot \mathbf{M}_v^1 \right] dS, \\
 B_{v\mu}^{12} &= \frac{jk_s^2}{\pi} \int_S \left[(\mathbf{n} \times \mathcal{N}_\mu^1) \cdot \mathbf{N}_v^1 + \sqrt{\frac{\varepsilon_i}{\varepsilon_s}} (\mathbf{n} \times \mathcal{M}_\mu^1) \cdot \mathbf{M}_v^1 \right] dS, \\
 B_{v\mu}^{21} &= \frac{jk_s^2}{\pi} \int_S \left[(\mathbf{n} \times \mathcal{M}_\mu^1) \cdot \mathbf{M}_v^1 + \sqrt{\frac{\varepsilon_i}{\varepsilon_s}} (\mathbf{n} \times \mathcal{N}_\mu^1) \cdot \mathbf{N}_v^1 \right] dS, \\
 B_{v\mu}^{22} &= \frac{jk_s^2}{\pi} \int_S \left[(\mathbf{n} \times \mathcal{N}_\mu^1) \cdot \mathbf{M}_v^1 + \sqrt{\frac{\varepsilon_i}{\varepsilon_s}} (\mathbf{n} \times \mathcal{M}_\mu^1) \cdot \mathbf{N}_v^1 \right] dS,
 \end{aligned} \tag{18}$$

and

$$\begin{aligned}
 A_{0v\mu}^{11} &= \int_S \left[(\mathbf{n} \times \mathbf{M}_\mu^1) \cdot \mathcal{M}_v^3 + (\mathbf{n} \times \mathbf{N}_\mu^1) \cdot \mathcal{N}_v^3 \right] dS, \\
 A_{0v\mu}^{12} &= \int_S \left[(\mathbf{n} \times \mathbf{N}_\mu^1) \cdot \mathcal{M}_v^3 + (\mathbf{n} \times \mathbf{M}_\mu^1) \cdot \mathcal{N}_v^3 \right] dS, \\
 A_{0v\mu}^{21} &= \int_S \left[(\mathbf{n} \times \mathbf{M}_\mu^1) \cdot \mathcal{N}_v^3 + (\mathbf{n} \times \mathbf{N}_\mu^1) \cdot \mathcal{M}_v^3 \right] dS, \\
 A_{0v\mu}^{22} &= \int_S \left[(\mathbf{n} \times \mathbf{N}_\mu^1) \cdot \mathcal{N}_v^3 + (\mathbf{n} \times \mathbf{M}_\mu^1) \cdot \mathcal{M}_v^3 \right] dS,
 \end{aligned} \tag{19}$$

respectively.

6 Acknowledgement

We gratefully acknowledge support of this work by Deutsche Forschungsgemeinschaft (DFG).

7 References

- [1] Kommission Reinhaltung der Luft: *Sicherer Umgang mit Fasermaterialien*, VDI Berichte 1417, VDI Verlag GmbH, Düsseldorf **1998**.
- [2] N. Höfert, C. Lehmann, M. Sharafi: Zweiter VDI-Ringversuch ‘‘Auswertung von Meßfiltern nach VDI 3492’’, *Gefahrstoffe – Reinhalt. Luft* **1999**, 59, 193–197.
- [3] K. Bauckhage, M. Bottlinger, F. Ebert, H. Fissan, S. Ripperger, K. Sommer, R. Weichert, T. Wriedt: Untersuchungen zur Charakterisierung von Faserkollektiven, in *Sicherer Umgang mit Fasermaterialien*, VDI Berichte 1417 (Eds. Kommission Reinhaltung der Luft), VDI Verlag, Düsseldorf, **1998**, 251–273.
- [4] H. Barthel: *Entwicklung eines Streulichtmeßverfahrens zur on-line Größenanalyse von inhalierbaren Faserstäuben*, Dissertation, Universität Kaiserslautern, **1999**.
- [5] J. List: *Identifikation und Charakterisierung von Fasern in der Luft*, Dissertation, Technische Universität Clausthal, **2002**.
- [6] M. I. Mishchenko, J. W. Hovenier, L. D. Travis: *Light Scattering by Nonspherical Particles: Theory, Measurements and Applications*, Academic Press, San Diego, **2000**.
- [7] E. Eremina, Y. Eremin, T. Wriedt: Extension of Discrete Sources Method to light scattering by highly elongates finite cylinders, *J. Modern Optics* **2004**, 51, 423–435.
- [8] A. Doicu, Y. Eremin, T. Wriedt: *Acoustic & Electromagnetic Scattering Analysis using Discrete Sources*, Academic Press, San Diego, **2000**.
- [9] C. Hafner, K. Bomholt: *The 3D electrodynamic wave simulator*, Wiley, Chichester, **1993**.
- [10] R. Schuh, T. Wriedt: Light scattering by bent cylindrical fibers for fiber length and diameter characterization, *Part. Syst. Char.* **2003**, 20, 243–249.